Predicting the location of weld line in microinjection-molded polyethylene via molecular orientation distribution

Predicting the Location of Weld Line in Microinjection Molded Polyethylene via Molecular Orientation Distribution

Tao Liao[1, 2], Xintong Zhao[1, 3], Xiao Yang[1, 3], Ben Whiteside[4], Phil Coates[4], Zhiyong Jiang[1*], Yongfeng Men[1, 2, 3*]

[1] State Key Laboratory of Polymer Physics and Chemistry, Changchun Institute of Applied Chemistry, Chinese Academy of Sciences, University of Chinese Academy of Sciences, Renmin Street 5625, Changchun 130022, P. R. China

[2] University of Chinese Academy of Sciences, Beijing 100049, P. R. China

[3] University of Science and Technology of China, Hefei 230026, P. R. China

[4] Faculty of Engineering and Informatics, University of Bradford, Bradford BD7 1DP, U.K.

Corresponding author: jiangzhy@ciac.ac.cn (Z. Jiang), men@ciac.ac.cn (Y. Men)

ABSTRACT

The microstructure and molecular orientation distribution over both the length and the thickness of microinjection molded linear low density polyethylene (LLDPE) with a weld line were characterized as a function of processing parameters using small angle X-ray scattering (SAXS) and wide angle X-ray diffraction (WAXD) techniques. The weld line was introduced via recombination of two separated melt streams with an angle of 180^{o} to each other in injection molding. The lamellar structure was found to be related to the mold temperature strongly but the injection velocity and the melt temperature slightly. Furthermore, the distributions of molecular orientation at different molding conditions and different positions in the cross-section of molded samples were derived from Hermans equation. The degree of orientation of polymeric chains and the thickness of oriented layers decrease considerably with an increase of both mold temperature and melt temperature, which could be explained by the stress relaxation of sheared chains and the reduced melt viscosity, respectively. The level of molecular orientation was found to be lowest in the weld line when varying injection velocity, mold temperature, and melt temperature, thus providing an effective means to identify the position of weld line induced by flow obstacles during injection molding process.

KEYWORDS: SAXS; microinjection molding; weld line; polyethylene; molecular orientation

INTRODUCTION

Nowadays, micromolding techniques, e.g., hot embossing, thermoforming, reaction injection molding, and microinjection molding, are being widely used with the rapid development of microelectromechanical-system (MEMS) or microsystem technology (MST). Typically, microinjection molding is a good candidate for industrial shaping operations due to its mass production ability, short cycle time, easiness for automation, and precise dimensional control.[1-3] However, as in the conventional injection molding, the defects, such as short shots, air traps, inhomogeneous shrinkage, and weld line, always occur in the final product during microinjection molding process, which are disadvantageous to the high repeatability and quality requirement of samples. Among these defects, the weld line is generally formed when two or more melt flows contact with each other immediately after the cooling process. This phenomenon is likely to appear in the products with a relatively complicated outline shape during melt processing of polymers. Besides, the raw polymeric materials may possess local heterogeneities of micrometer size, e.g., catalyst residues, which act as a barrier in the polymer melt thus separating the melt and forming the weld line as the separated melts meet. The existence of weld line dramatically reduces the bulk strength of polymeric goods due to the weak bonding at the interface of the weld line and the localized stress concentration around the V-notch defect.[4] Therefore, many studies relevant to the weld line in conventional injection molding have been conducted to unravel the molecular mechanism of weld line formation,[4,5] the morphology of the weld line,[6,7] and its effect on the mechanical properties.[8,9] Concerning the weld line in the microinjection molding, numerous researchers have studied the influence of processing conditions on the mechanical properties, and found that the tensile strength of welded products increases at elevated injection speeds and packing pressures.[10,11] In addition, the tensile strength of injection molded nylon 6 nanocomposite first increases and then deceases with increasing mold temperature and melt temperature for thin parts of 1 mm, whereas thick parts of 2.5 mm exhibit the positive melt and mold temperature dependence of the tensile strength. This thickness dependence of tensile strength was attributed to the different molecular orientation.[10] Apart from the processing parameters, the cross

section shape as an external factor can also affect the strength of the sample with a weld line. The strongest strength of weld line bar comes from equilateral triangle cross section, followed by the trapezoid and semi-circle shape.[12] This behavior was related to the ratio of perimeter and area of cross section shape. The higher the ratio, the stronger weld line strength would be. On the other hand, because the tensile strength of polymers is dependent on the inner structures, including skin-core structure and degree of orientation of molecular chains,[13] the molecular orientation at the weld line plays an important role in the mechanical properties of injection molded samples. Many characterization methods have been employed to probe molecular orientation at the weld line region. Soft X-ray photography[14] and transmitted photomicrographs[15] were used as indirect approaches to investigate the fiber orientation of weld line parts in the fiber reinforced plastic under the microinjection molding. Considering the simulation method, the finite element method was also applied to study the different fiber orientation along the flow direction and between skin layer and core layer.[16] The results from these approaches indicated that fibers take orientation toward flow direction in the center part between the gate and the weld line, whereas fibers are oriented almost perpendicular to the flow direction at the weld line owing to the fountain flow feature.[14] It was also reported that the back-flow occurring at the weld line area changes the fiber orientation from parallel to perpendicular to the weld line.[17] In addition, Tomari et al.[18] utilized Fourier transform infrared spectroscopy (FTIR) to characterize the molecular orientation of liquid crystal polymer (LCP) and polycarbonate (PC) at weld line region, and found that LCP molecules at weld line region are oriented along the thickness direction while PC molecules are in random orientation independent of the weld line. Furthermore, X-ray measurements were proved to be a powerful tool to reveal the local molecular orientation in microinjection molded sample. Shi et al.[19] calculated the level of orientation of polymeric chains in molded polyethylene samples using small angle X-ray scattering (SAXS) and wide angle X-ray diffraction (WAXD), and found a larger molecular orientation in high-molecular-weight high density polyethylene (HMW-HDPE) than in low-molecular-weight high density polyethylene (LMW-HDPE), which was considered to be responsible for the higher tensile strength of the HMW-HDPE

specimen. Healy et al.[20] utilized SAXS and WAXD to examine the residual chain orientation in microinjection molded linear polyethylene, and unravelled that it is the oriented crystal growth instead of residual chain orientation that contributes to the majority of the orientation. Granlund et al.[21,22] mapped the two dimensional chain orientation distribution in the cross section parallel and perpendicular to the flow direction in injection molded talc-reinforced isotactic polypropylene using the raster scanning SAXS and WAXD, and indicated the structural heterogeneities and asymmetries as a result of lateral temperature gradient across the mold. Ulcer et al.[23] applied matrixing micro beam X-ray diffraction and transmission optical photomicrographs to analyze the structure at the weld region of poly(arylene ether ketone), and revealed that the sample exhibits a multilayer structure at the weld line region. Nevertheless, a full picture regarding the orientation distribution of polymeric chains around the weld line region has not yet been established quantitatively in the microinjection molded sample.

Since the weld line can significantly lower the mechanical strength of injection molded polymer products, it is vital to clarify the position of weld line and also to provide possible routes for prevention of the weld line formation in injection molding. The present study aims to explore the influence of molding parameters on the microstructure and identify the structural feature of weld line in microinjection molded samples by means of positional scanning WAXD and SAXS techniques. For this purpose, linear low density polyethylene (LLDPE) samples with a weld line are prepared under different processing parameters via recombination of the two melt streams in the opposite direction. Thereafter, the structural and morphological evolution of molded LLDPE samples at the molecular and nanometric length scales are investigated as a function of injection molding parameters and sample position, e.g., flow direction and thickness direction. As will be illustrated in the following sections, the degree of orientation of molecular chains is found to be lowest in the weld line, irrespective of processing conditions.

EXPERIMENTAL SECTION

The commercial LLDPE pellets used in this study was supplied by ExxonMobil

Chemical Company. The molecular weights were M_w = 6.20×10^4 g/mol and M_n = 1.72×10^4 g/mol, and the melt flow index was 20 g/10 min. The crystallinity of the raw material was ca. 0.37 as determined from the DSC melting scan (Mettler Toledo Instruments). The pellets were injection molded into dumbbell-shaped bars using a microinjection molding machine (Wittmann Battenfeld Microsystem 15, Austria), yielding strips with a dimension of 14.44 (length) × 0.56 (width) ×0.25 (thickness) mm^3. When each molding cycle was accomplished, we fetched the sample and used a copper brush to remove the residual polymer melts on the mold completely. Weld lines were formed in the samples when two separated melt streams recombined head to head at approximate 180^o to each other. Three molding parameters, including mold temperature, melt temperature, and injection velocity, were varied during injection molding process as shown in Table 1. The samples used for WAXD and SAXS measurements were schematically represented in Figure 1.

SAXS and WAXD (transmission mode) were performed simultaneously on a Nano-inXider (Xenocs, France) with the wavelength of X-ray radiation being 0.154 nm. The distances between sample and detector were 937.50 mm and 75.25 mm for SAXS and WAXD, respectively. The dimension of the X-ray beam at the sample position was 200 × 200 μm^2. The microinjection molded sample was mounted onto a two-dimensional translational stage, and was then moved stepwise in such a way that the incident X-ray beam scanned over the neck shoulder along the flow direction. The two dimensional patterns were collected at selected positions with an acquisition time of 1000 seconds by a Pilatus 100 K detector (resolution: 487 × 195). The scattering data were first normalized with respect to the primary beam intensity and then were calibrated for background scattering using the software of "Fit2D". One-dimensional SAXS curves were obtained from SAXS patterns via a narrow rectangular integration along the melt flow direction, and azimuthal intensity distributions of the (110) lattice plane were also extracted from the inner cycle of WAXD patterns.

Furthermore, positional scanning WAXD measurements were carried out on a modified Xeuss system (Xenocs, France) with the micro-focus beam size of 50 x 50 μm^2 at the sample position. The wavelength of the X-ray radiation was 0.154 nm, and the sample

to detector distance was 28.6 mm. In order to map the morphological distribution along the thickness direction, strips with a breadth of ca. 0.2 mm were cut from the middle of molded samples along the flow direction, and five different scanning layers with an interval of ca. 0.05 mm were chosen in the thickness direction, as shown in Figure 1. The thickness of each scanning layer was almost equivalent to the X-ray spot size of 0.05 mm. At each equal distance from the sample surface, WAXD images were recorded by scanning over the rectangular strips along the flow direction from one cavity gate to the other with a step length of 200 μm. The two-dimensional WAXD patterns were collected within 60 seconds with a Pilatus 100 K detector. The background scattering was then subtracted from the recorded diffraction patterns, and azimuthal intensity distributions were obtained from the respective (*hkl)* lattice plane of the normalized patterns.

In order to determine the weld line location directly, an Olympus BX41 polarized optical microscopy (POM) was applied to visualize the morphology of weld line regions in the molded samples. Additionally, mechanical measurements of welded samples were carried out on a custom-made tensile testing machine (Care, Tianjin, China). The tensile results were obtained at room temperature with a constant crosshead speed of 0.02 mm/s.

Table 1 The processing parameters for the microinjection molding. The mold temperature was varied under a melt temperature of 180 ºC and an injection velocity of 200 mm/s; the melt temperature was changed as the mold temperature was fixed at 50 ºC and injection velocity at 200 mm/s; the injection velocity was varied as the mold and melt temperature were preset at 22 and 180 ºC, respectively.

Mold temperature (ºC)	22, 50, 75, 100
Melt temperature (ºC)	140, 160, 180
Injection velocity (mm/s)	200, 500, 800
Injection pressure (bar)	160
Hold pressure (bar)	250
Cooling time (s)	10

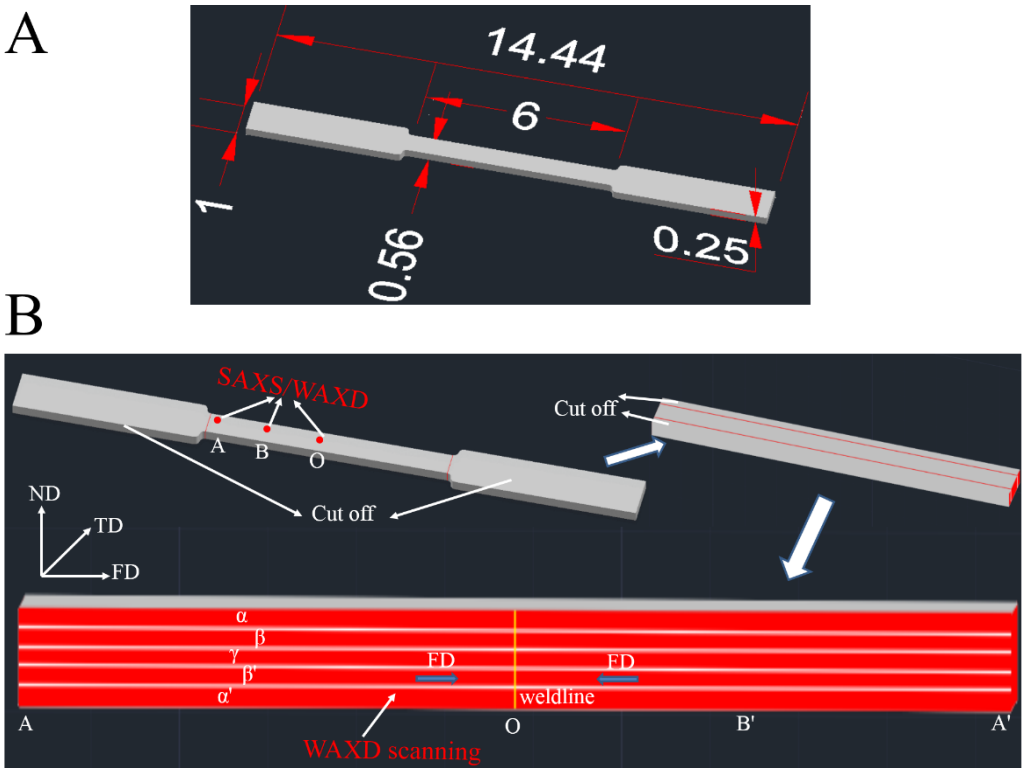

Figure 1 Dimensions (the unit is millimeter) of the microinjection molded sample bar (A) and schematic representation of the molded sample used for SAXS and WAXD measurements (B). Three selected positions where the incident X-ray beam irradiates are shown in the figure. The direction of the incident beam is parallel to the normal direction for SAXS/WAXD measurements. For scanning WAXD experiments, strips with a breadth of ca. 0.2 mm are cut from the middle of specimens along the flow direction and the direction of X-ray is along the transverse direction. FD, TD, and ND represent the flow direction, transverse direction, and normal direction, respectively. The position where the weld line is formed in the molded sample is designated as "O".

RESULTS AND DISCUSSION

SAXS and WAXS Results

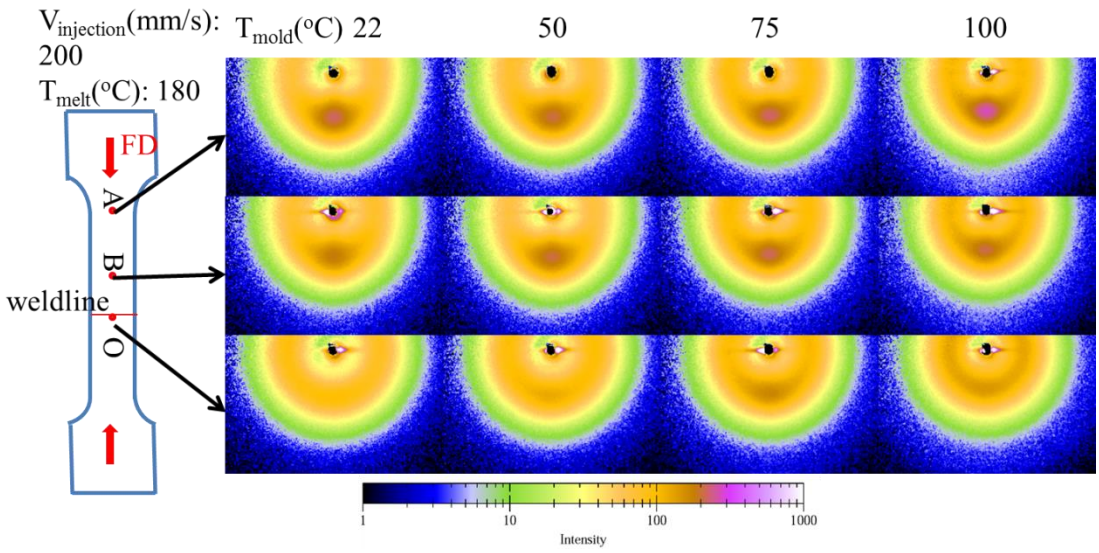

Figure 2 Selected two-dimensional SAXS patterns of injection-molded samples measured at different positions (vertical direction) and different mold temperatures (horizontal direction). The samples are produced at an injection velocity of 200 mm/s and a melt temperature of 180 °C. The flow direction is vertical.

In order to elucidate the distribution of lamellar structure along the flow direction, SAXS patterns were recorded in normal direction with the incident beam passing through the complete thickness, and the results are shown in Figure 2. Three typical points were selected in the present case, i.e., a position close to the injection molding gate (A), in the middle of the sample (O), and in between the above two cases (B). It should be noted that the point O is the geometric center of the sample bars, which is not necessarily the position of weld line. As presented evidently in Figure 2, the SAXS patterns become less anisotropic with increasing distance from the injection gate at corresponding mold temperatures. This behavior means that the orientation of crystalline lamellae decreases gradually along the injection flow direction as a result of reduced shear stress effect in the polymer. On the other hand, an overall increase in the scattering intensity is observed as the mold temperature increases, which is due to the growing electron density contrast between the lamellae and the amorphous layers formed at elevated temperatures during molding process. In addition, the azimuthal width of the scattering intensity maximum increases distinctly upon increasing mold

temperature, which can be attributed to a relaxation of lamellar orientation to a larger extent at elevated temperatures.

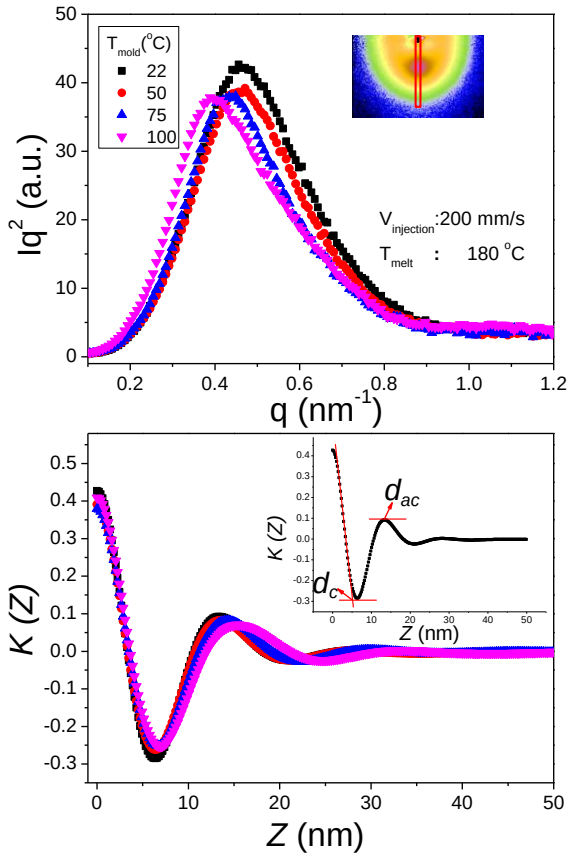

Figure 3 Plots of Lorentz-corrected one dimensional SAXS intensity distributions of molded samples at the position of A against mold temperature (top) and their corresponding correlation functions (bottom). The insets show how the one dimensional scattering intensity distribution curves along the flow direction (top), as well as the long period d_{ac} and the crystalline thickness d_c are obtained (bottom).

Furthermore, the average thickness of the crystalline and amorphous layers measured along the injection flow direction can be obtained from the one-dimensional scattering intensity distribution via inverse Fourier transform:[24,25]

$$K(z) = \frac{\int_0^\infty I(q)q^2 \cos(qz)dq}{\int_0^\infty I(q)q^2 dq} \quad (1)$$

Because the crystallinity as determined from DSC measurement is lower than 0.5 for the sample, the smaller value in the correlation function can be safely assigned to the average thickness of lamellae. The values of the long period d_{ac}, the crystalline

thickness d_c, and the amorphous thickness d_a for samples prepared at different molding conditions are demonstrated in Figure 4. The linear crystallinity, representing the volume fraction of crystalline lamellae along the melt flow direction, was evaluated by the relation d_c/d_{ac}, and the results are displayed in Figure 5. It can be seen from Figure 4 and Figure 5 that these parameters at the lamellar level are not much affected by the injection velocity, melt temperature, and position of injection-molded samples. However, the long period increases evidently with increasing mold temperature, which is mainly caused by an increase of the average thickness of amorphous phase. The lamellar thickness increases only slightly with an increase of mold temperature. This behavior stems from the presence of short side chain branches in the LLDPE sample, which restricts the lamellar thickening upon high temperature crystallization to a large extent. In addition, the linear crystallinity decreases obviously at high mold temperatures (e.g., 100 °C), which is caused by a faster growth of the average thickness of amorphous layers.

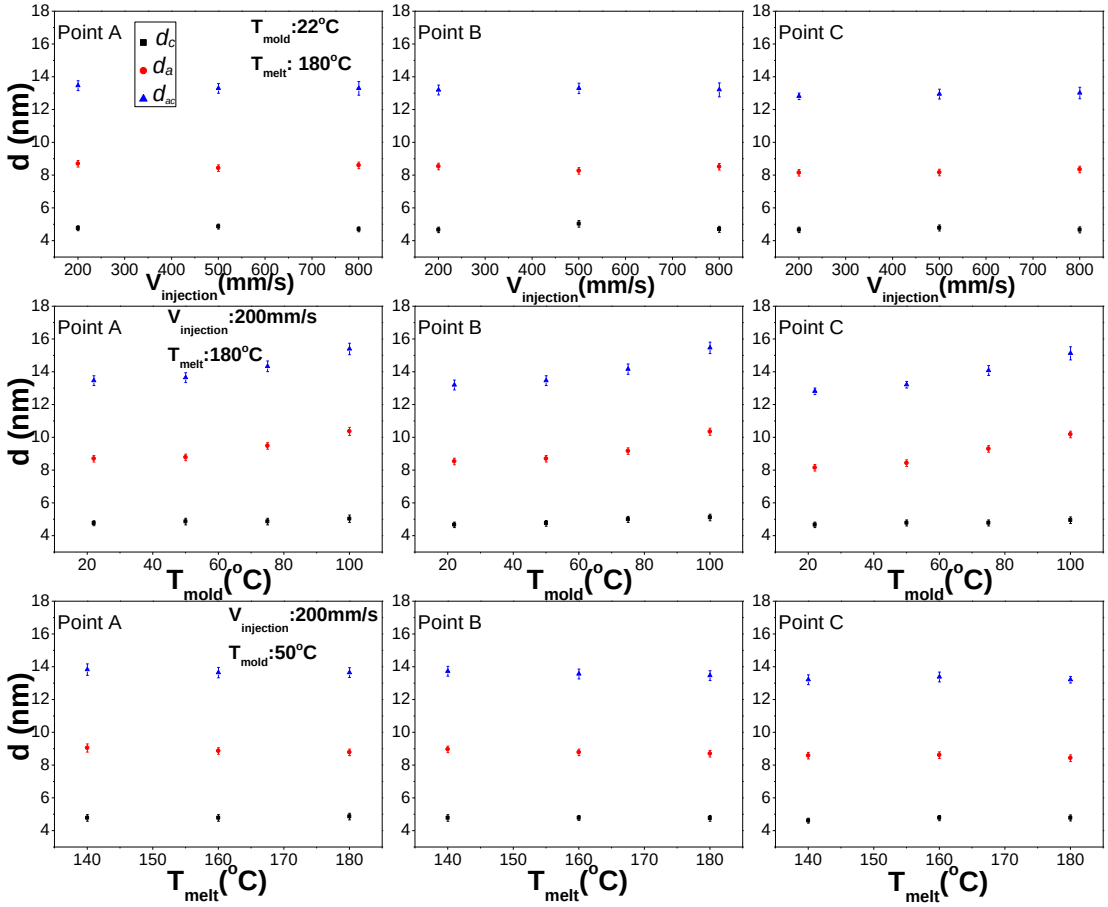

Figure 4 Variations of the long period (d_{ac}), and the average thickness of lamellar (d_c)

and amorphous layers (d_a) with injection velocity (top row), mold temperature (middle row), as well as melt temperature (bottom row) measured for samples with a weld line at three selected positions. The processing conditions are illustrated in the inset of each plot.

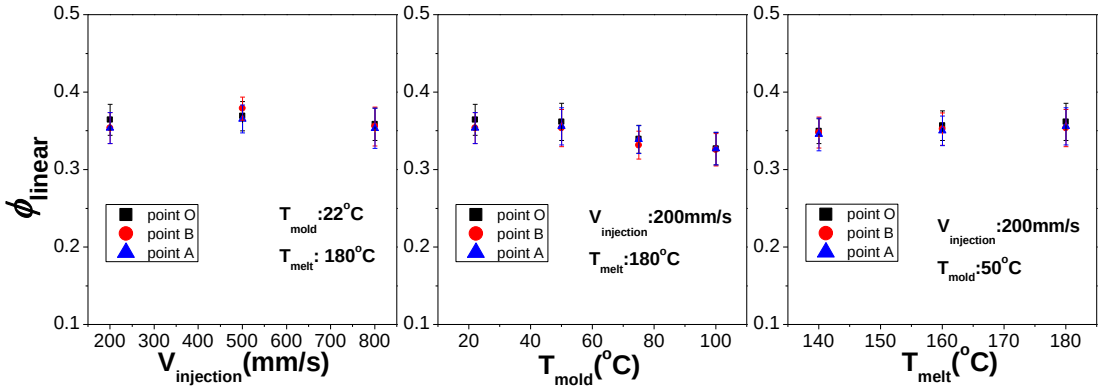

Figure 5 Variations of the linear crystallinity φ_{linear} (d_c/d_{ac}) with injection velocity (left), mold temperature (middle), and melt temperature (right) measured for molded samples at three selected positions.

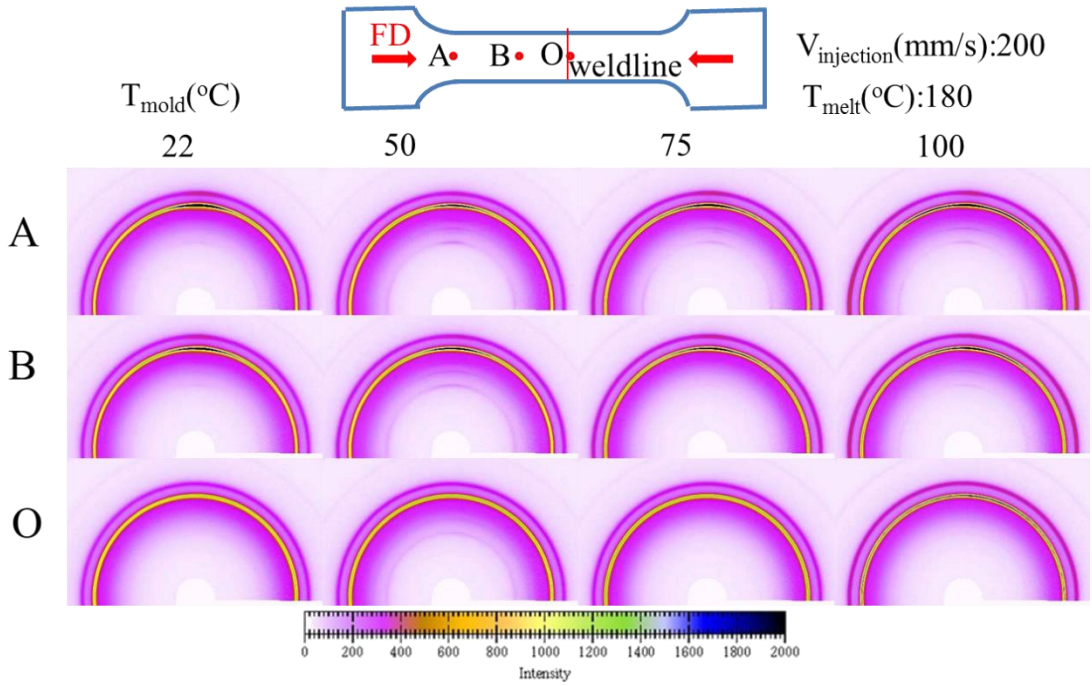

Figure 6 Selected two-dimensional WAXD patterns of injection-molded samples taken at different positions (vertical direction) and different mold temperatures (horizontal direction). The samples are shaped at an injection velocity of 200 mm/s and a melt temperature of 180 °C. The flow direction is horizontal.

The texture of injection-molded samples at the crystal lattice level was probed along the flow direction by WAXD measurements, and selected WAXD patterns are shown as a function of mold temperature and distance from the gate in Figure 6. The two Debye peaks in the WAXD patterns correspond to the (110) (inner) and (200) (outer) lattice planes of the orthorhombic form of polyethylene, respectively. It is evident that the WAXD patterns transform from a diffraction diagram with peaks on the equator (i.e., perpendicular to the flow direction) to a nearly isotropic diffraction intensity distribution upon approaching to the weld line, irrespective of mold temperature. This behavior indicates a low degree of orientation of the polymeric chains in the position of weld line. On the other hand, a broad diffraction maximum especially for (110) reflection is observed when the mold temperature is increased. This fact implies a considerable relaxation of stretched chains and thus a lower orientation of the chains in the crystallites on molding at high temperatures. In order to characterize the degree of orientation of molecular chains quantitatively, azimuthal intensity distribution curves of the (*hkl*) lattice plane $I(\mu)$ were obtained and an orientational order parameter proposed by Hermans was assessed with the following equation:[26]

$$S_{hkl} = \frac{3<\cos^2\varphi_{hkl}>-1}{2} \quad (2)$$

where $<\cos^2\varphi_{hkl}>$ is expressed as

$$<cos^2\varphi_{hkl}>=\frac{\int_0^{\pi/2} I_{hkl}(\varphi)sin\varphi cos^2\varphi d\varphi}{\int_0^{\pi/2} I_{hkl}(\varphi)sin\varphi d\varphi} \quad (3)$$

and $\cos\varphi_{hkl}$ is calculated by applying Polanyi equation:[27]

$$\cos\varphi_{hkl} = cos\theta_{hkl}cos\mu \quad (4)$$

where φ_{hkl}, θ_{hkl}, and μ represent the angle between the normal vector of (*hkl*) lattice plane and the flow direction, the Bragg scattering angle, and the azimuthal angle, respectively. In the case of the plane with its normal ideally perpendicular to the flow direction, the orientational order parameter would be -0.5. If the normal of the plane is parallel to the flow direction, the orientational order parameter S_{hkl} = 1, while the polymeric chains are randomly oriented in the sample, S_{hkl} is set to 0. The azimuthal

scans along the (110) reflection are given in Figure S1, and the results for the orientational order parameter of (110) plane are shown as a function of position and processing condition of molded samples in Figure 7.

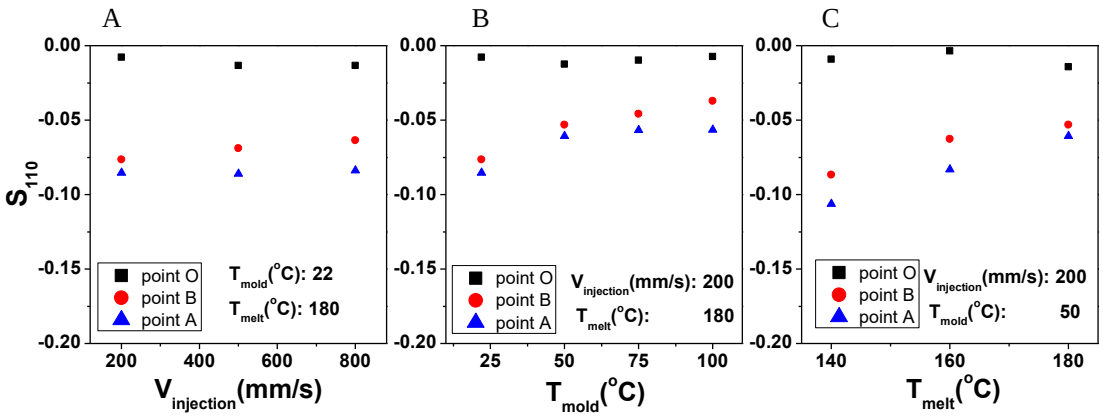

Figure 7 Evolution of the orientational order parameters of (110) reflection measured for injection-molded samples at different injection velocities (A), mold temperatures (B), and melt temperatures (C).

It is to be noted that the value of S_{110} increases significantly along the melt flow direction and is approximate to zero at the position of weld line when varying injection velocity, mold temperature, as well as melt temperature. This behavior means that the molecular chains in the crystalline phase are oriented to a less extent with increasing distance from the gate and tend to be isotropic distribution at the weld line position. As was found, the degree of orientation of molecular segments at points "A" and "B" is affected by injection velocity only slightly. This finding can be tentatively explained in the following two aspects. On one hand, a higher injection flow rate results in a higher shear stress in the melt and hence increases the level of orientation of molecular chains. On the other hand, an increase in the injection speed would also reduce the time that the polymer melt undergoes strong shear stress during the filling stage,[23] leading to the chains oriented to a lesser degree. In contrast, the molecular orientation is influenced by mold temperature and melt temperature quite strongly at both positions of "A" and "B". As it appears, the degree of orientation of chains in the crystallites decreases gradually with increasing mold temperature. This fact is ascribed to the sufficient

relaxation of polymeric chains at higher ambient temperature upon molding process. Additionally, a higher melt temperature gives rise to a lower melt viscosity and therefore decreasing the level of orientation in the polymer.

Scanning WAXD Results

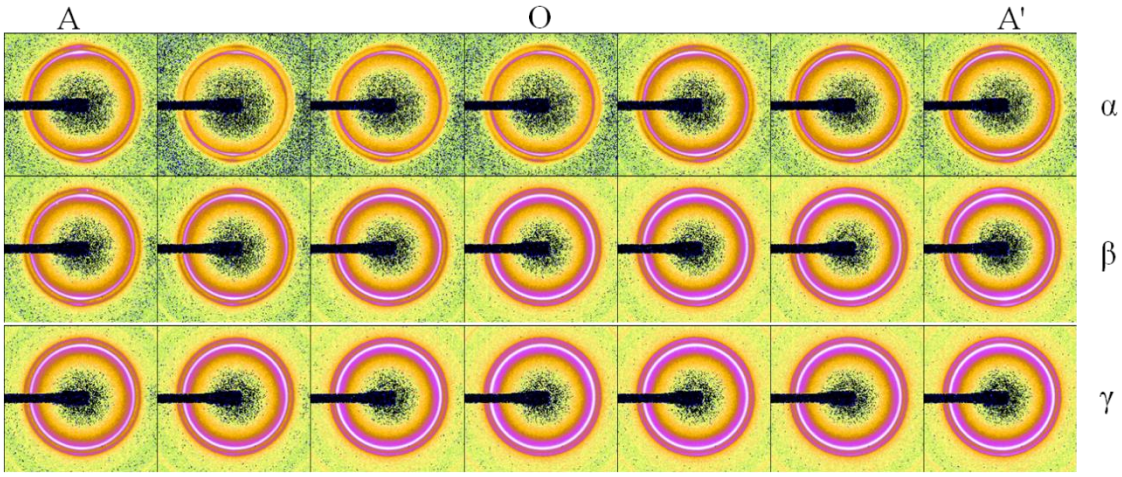

Figure 8 Selected wide angle X-ray diffraction patterns recorded at different positions in the cross section of injection-molded LLDPE sample with a weld line. α, β, and γ (from top to bottom) represent three structural layers taken from a position close to the surface to the middle of the sample, respectively.

It is well-known that the injection molded sample typically exhibits a skin-core structure because of shear rate gradient along the sample thickness direction. For the sake of addressing the distribution and structure of injection flow-induced orientations quantitatively, a scanning microfocus WAXD measurement was performed along the flow direction and the thickness of molded samples, respectively. The molded samples were decomposed into five layers along the thickness direction and were scanned along the flow direction from one gate to the other gate with a step size of 200 μm at each structural layer. Figure 8 gives the selected 2D WAXD patterns at different positions where scanning over half the thickness of the injection molded sample is presented. The sample was prepared under an injection flow velocity of 200 mm/s, a melt temperature of 180 ºC, and a mold temperature of 22 ºC, respectively. In the case of the structural layer close to the sample surface, the azimuthal widths of the two diffraction peaks become gradually broader when being scanned from the gate to the weld line, indicating

a reduction in the level of orientation of polymeric molecules. Another noticeable issue to be learned from Figure 8 is that the WAXD patterns transform from an apparently anisotropic scattering intensity distribution to two Debye diffraction rings with increasing distance from the edge (i.e., along the normal direction).

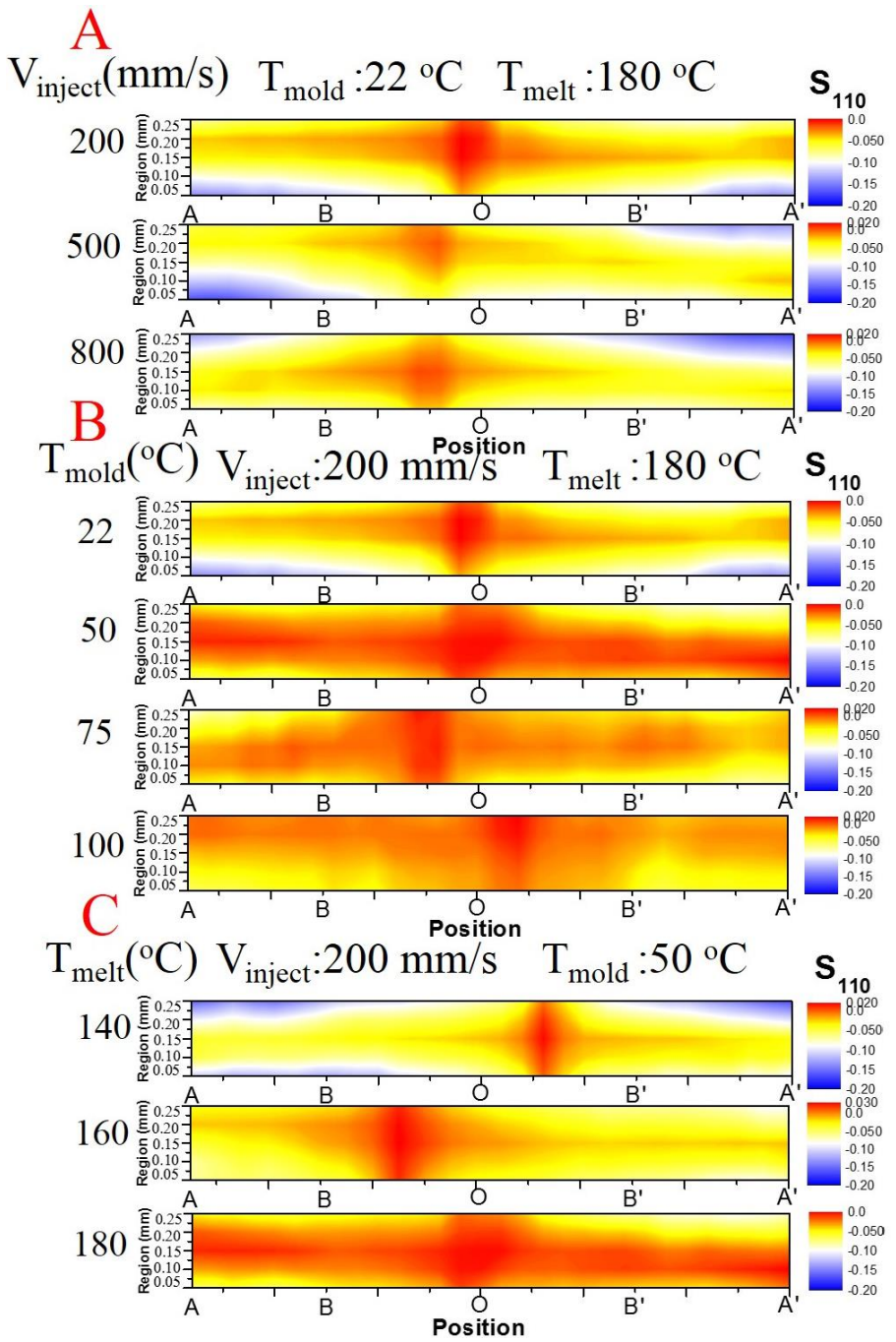

Figure 9 Contour profiles of the orientational order parameters associated with (110) reflection for the cross section of injection-molded samples produced at different injection velocities (A), mold temperatures (B), and melt temperatures (C). The molding conditions are indicated on each graph. The values in the ordinate denote the

distance from the sample surface along the thickness direction. About 150 WAXD patterns are recorded in the cross section of molded samples to map the contour profile.

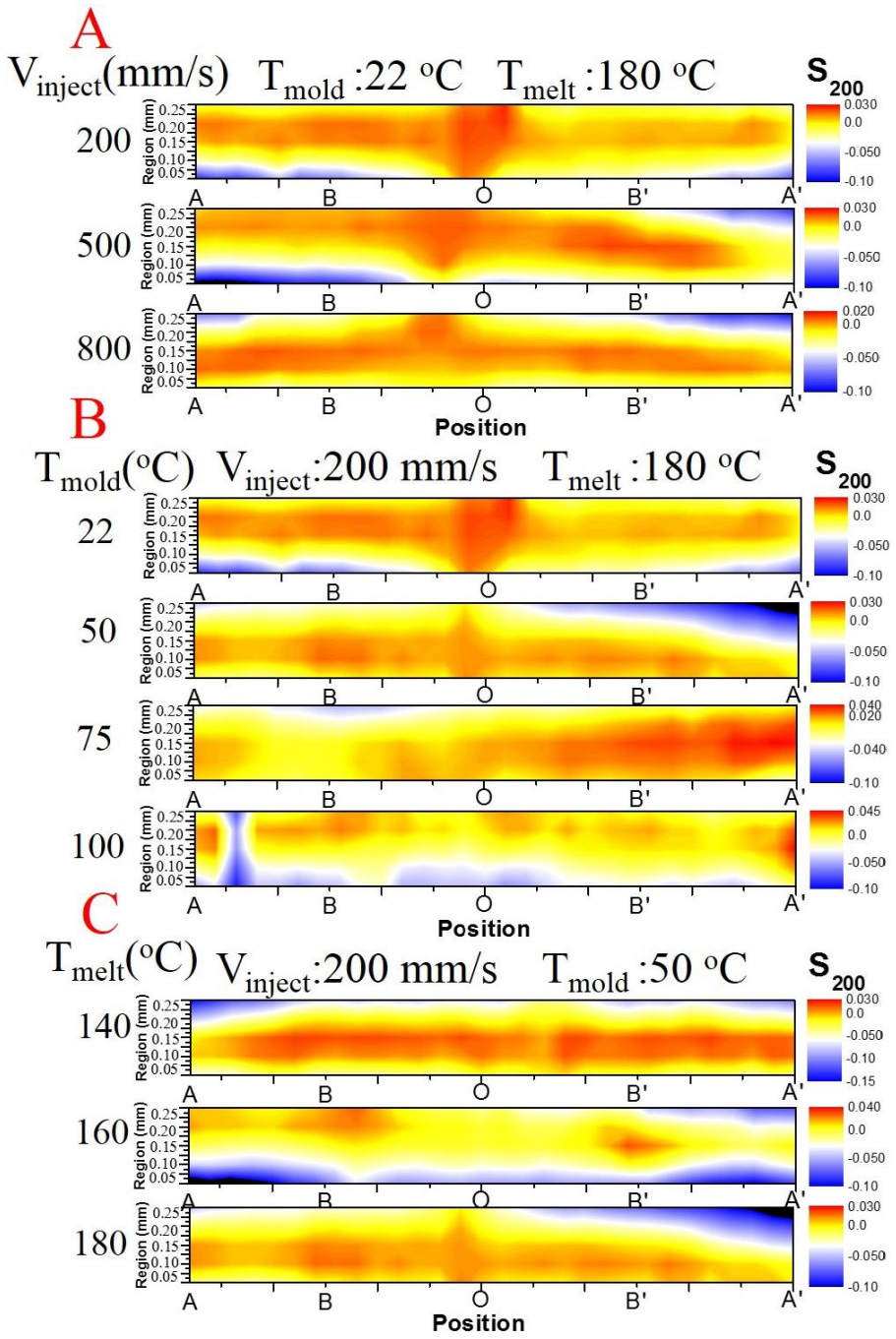

Figure 10 Contour profiles of the orientational order parameters associated with (200) reflection for injection-molded samples produced at different injection velocities (A), mold temperatures (B), and melt temperatures (C). The molding conditions are indicated on each graph.

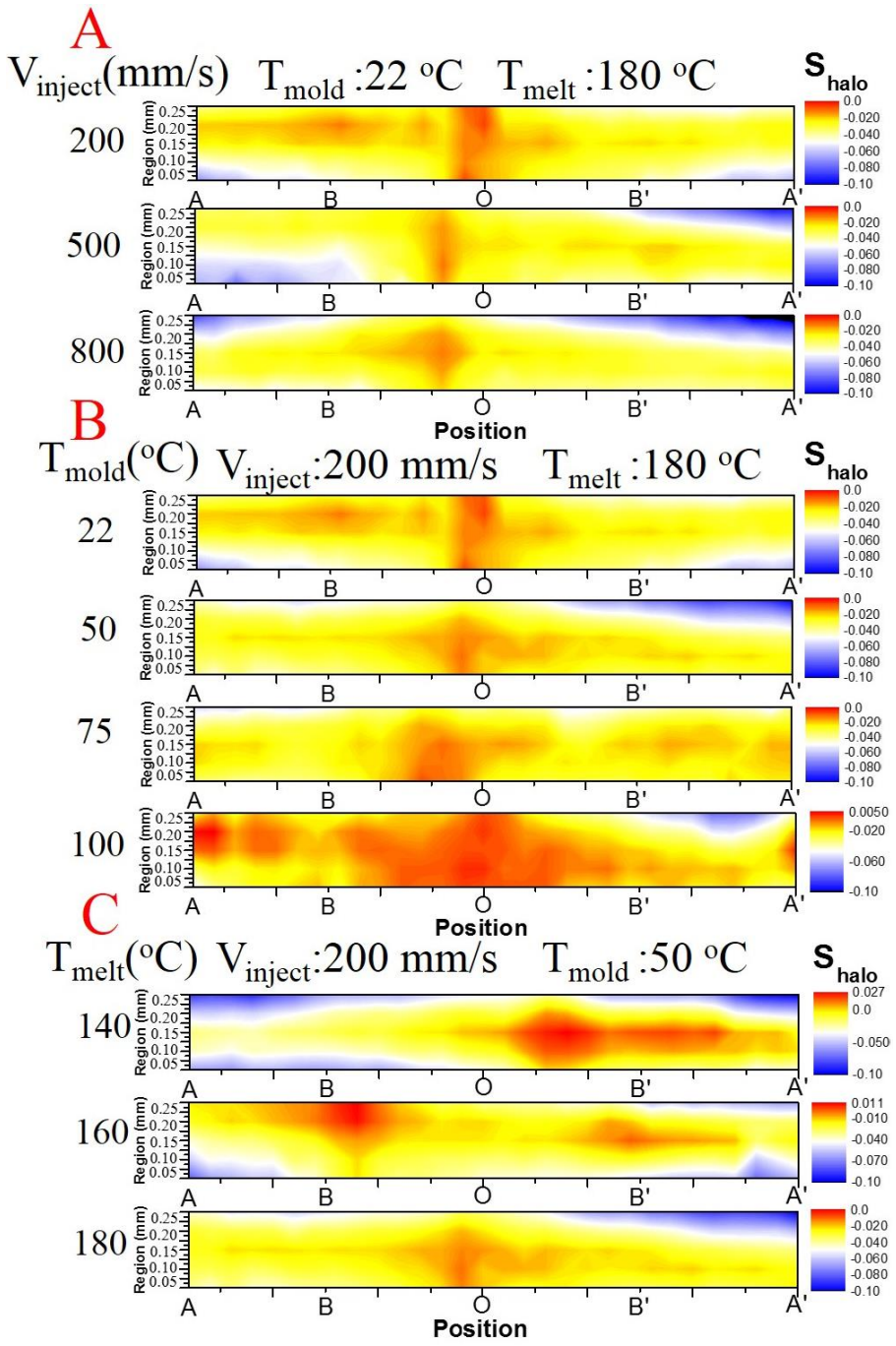

Figure 11 Contour profiles of the orientational order parameters associated with the amorphous halo for injection-molded samples produced at different injection velocities (A), mold temperatures (B), and melt temperatures (C). The molding conditions are indicated on each graph.

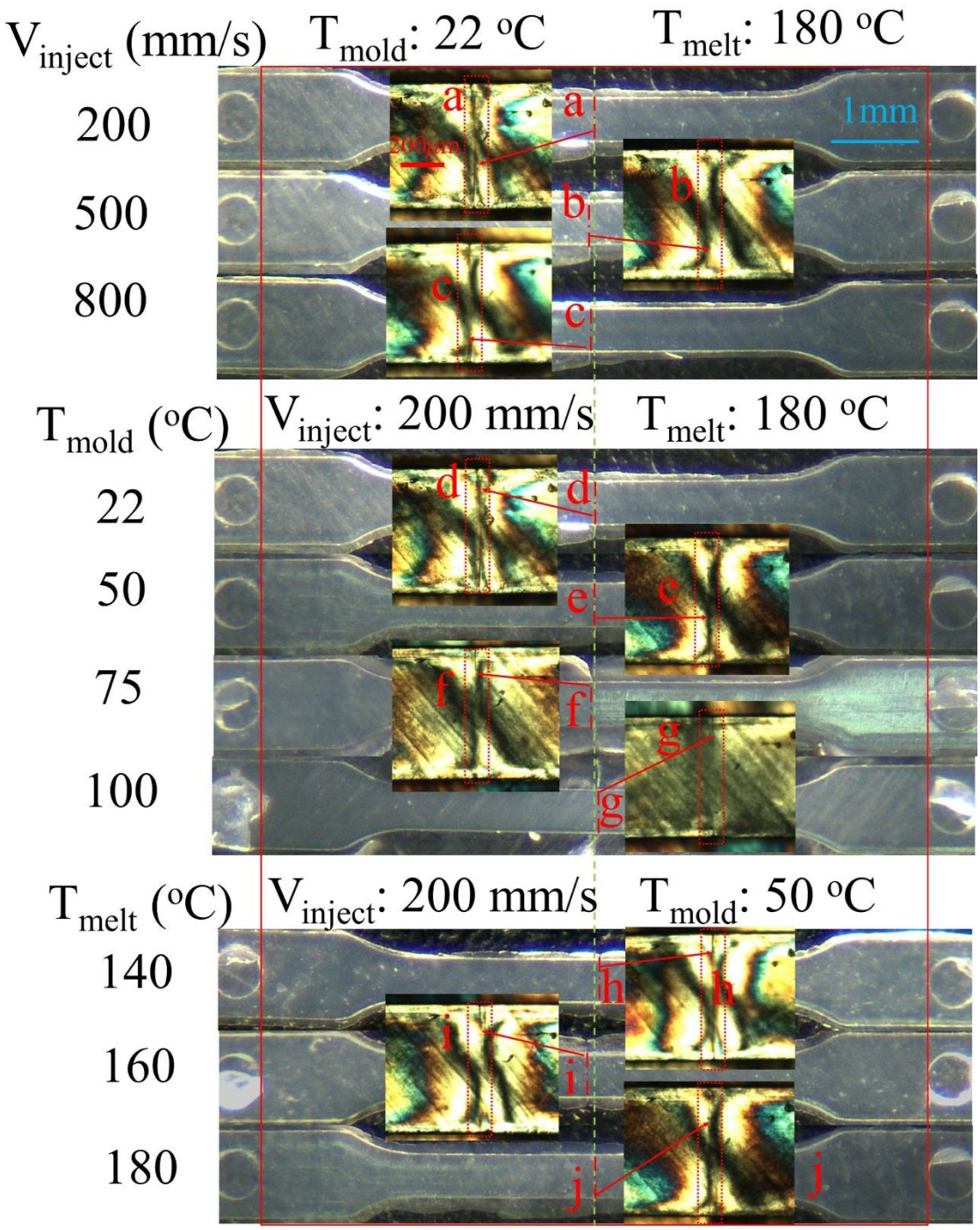

Figure 12 Optical micrographs taken at the weld line regions of injection-molded samples. The samples are produced at different injection velocities (top), mold temperatures (middle), and melt temperatures (bottom). The green dash line represents the geometric center of sample bars, and the red dash dot line denotes the position of weld lines as evidenced by optical micrographs.

Furthermore, the two dimensional contour profiles of the orientational order parameters

were derived from the azimuthal intensity distributions of (*hkl*) reflection according to the Hermans equation, and the results for the orientational order parameters associated with the (110) reflection, (200) reflection, and the amorphous halo are presented in Figure 9, Figure 10, and Figure 11, respectively. As can be seen, the spatial distribution of flow-induced orientation in the molded samples exhibits a clear red cross-shaped pattern, meaning the presence of a typical multilayer structure of skin and core layers. It is to be noted that the center of these cross stripes is located in the vicinity of the geometric middle of molded sample bars at which the weld line is expected to be. In some cases the cross stripes become less pronounced in the plots of Figure 10 and Figure 11 as compared to those observed in Figure 9, which can be ascribed to the relatively lower diffraction intensity of the (200) lattice plane and the amorphous halo and thus resulting in considerable calculation error. In order to check the reproducibility of these results, one molded sample was selected to repeat the scanning WAXD experiments and the results are indicated in Figure S2. One finds that there is still a cross stripe in the weld line, which is well consistent with the above mentioned results. On the other hand, polarized optical microscopy was used to observe the weld line location directly, and the results are displayed in Figure 12. A weld line can be visualized on the sample surface as a V-shaped notch in the optical micrographs. Compared to the results in Figure 9-11 and Figure 12, there exists a good coincidence between the weld line location as evidenced by microscopy and the red vertical streak in the contour profiles, regardless of injection molding conditions. This fact indicates that the orientation distribution of polymeric chains in the cross section of injection molded samples can be used to identify the position of the weld line. As a result, scanning microfocus WAXD technique is an effective means to monitor the position of local defects, such as weld line, which is initiated by microvoids and catalyst residues in the polymer melt during the practical industrial production process. In some cases, it is difficult to achieve a weld line directly in the center of the component for such a small test sample because it requires very accurate tooling and a well controlled process in order to achieve this. Actually, the weld line position deviates from part to part either side of the centerline, e.g., in Figure 9(C). If it was simply due to a slight geometric

difference in the mold cavity or a heating/cooling imbalance in the tool, one would expect the weld line to lie consistently on one side of the centerline. Nevertheless, this is not the case in the present work. One notes that the variability of the weld line location becomes smaller when the melt temperature is raised from 140 ºC to 180 ºC. These results, therefore, suggest an inconsistency in the temperature/viscosity in the material itself. Moreover, the effect of molding conditions on the structure distribution over both the thickness and the length of samples can also be elucidated from the contour profiles in Figure 9. Obviously, the thickness of oriented skin layers decreases progressively from the gate to the weld line along the melt flow direction. As the mold temperature is increased, the core layer is extended and spreads almost to the surface of the molded sample at a temperature of 100 ºC, resulting in an overall decrease of the molecular orientation. In addition, the total thickness of the oriented layers is found to decrease with increasing melt temperature because of a lower viscosity in the melt which makes the orientation of the polymeric chains more difficult. However, the change of oriented layer thickness with injection speed is less pronounced for the molded samples.

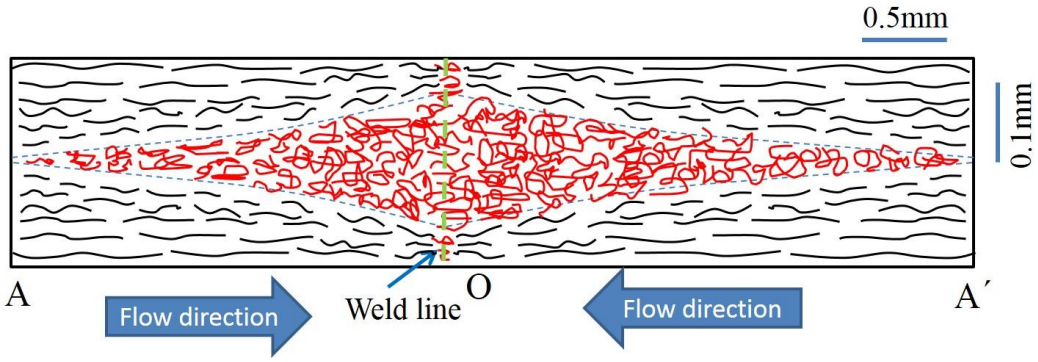

Figure 13 Schematic representation of the distribution of degree of orientation of molecular chains in the cross section of injection-molded sample with a weld line. The black and red curves denote the polymeric chains with a high and a low level of orientation, respectively. For the sake of clarity, positions along the flow direction and the thickness direction are marked by different scale bars as shown in the figure.

Another important finding observed in Figure 9 is that the molecular orientation is always lowest close to the weld line for each molded sample when varying injection velocity, mold temperature, and melt temperature. Figure 13 gives a schematic

representation of the molecular orientation distribution in the cross section of welded samples. This behavior could be traced back to the following reasons. First, the actual temperature of the site where the two melt fronts contact is relatively high (like a hot wall),[19] and thus the formation of the weld line is always accompanied by a substantial relaxation of the oriented chains upon molding process. Second, possible back flow[17] at the instant of contact of two melt streams also reduces the orientation of polymeric chains. Third, as two melt fronts just come into contact, polymeric chains in the two melt fronts can penetrate into each other at the flow interface via self-diffusion process because the free energy at the flow front is higher than that in other parts of the sample, thus gradually randomizing the orientation of chain segments to a certain degree.[5,6]

In order to reveal the relationship between microstructure and mechanical properties, tensile stretching measurements of the welded samples were performed. Nominal stress-strain curves are illustrated in Figure S3, and the resultant mechanical parameters, including elongation at break, the fracture toughness (the area under the whole stress-strain curve), the tensile modulus, as well as maximum stress, are summarized in Figure 14. One notes that these mechanical parameters are hardly impacted by the injection velocity, which is in line with the SAXS and WAXD results. However, the dependence of the mechanical parameters on the mold temperature and the melt temperature is clearly seen. Both the elongation at break and the fracture toughness increase with increasing mold temperature and melt temperature, which can be explained by a reduced degree of orientation of polymeric segments at high temperatures. Moreover, an overall increase in the tensile modulus and the maximum stress is observed when the mold temperature and melt temperature are elevated. Since the small-strain mechanical properties are dominated by the crystalline lamellae,[29] this dependence can be attributed to the larger ratio of core layer to skin layer as revealed by Figure 9.

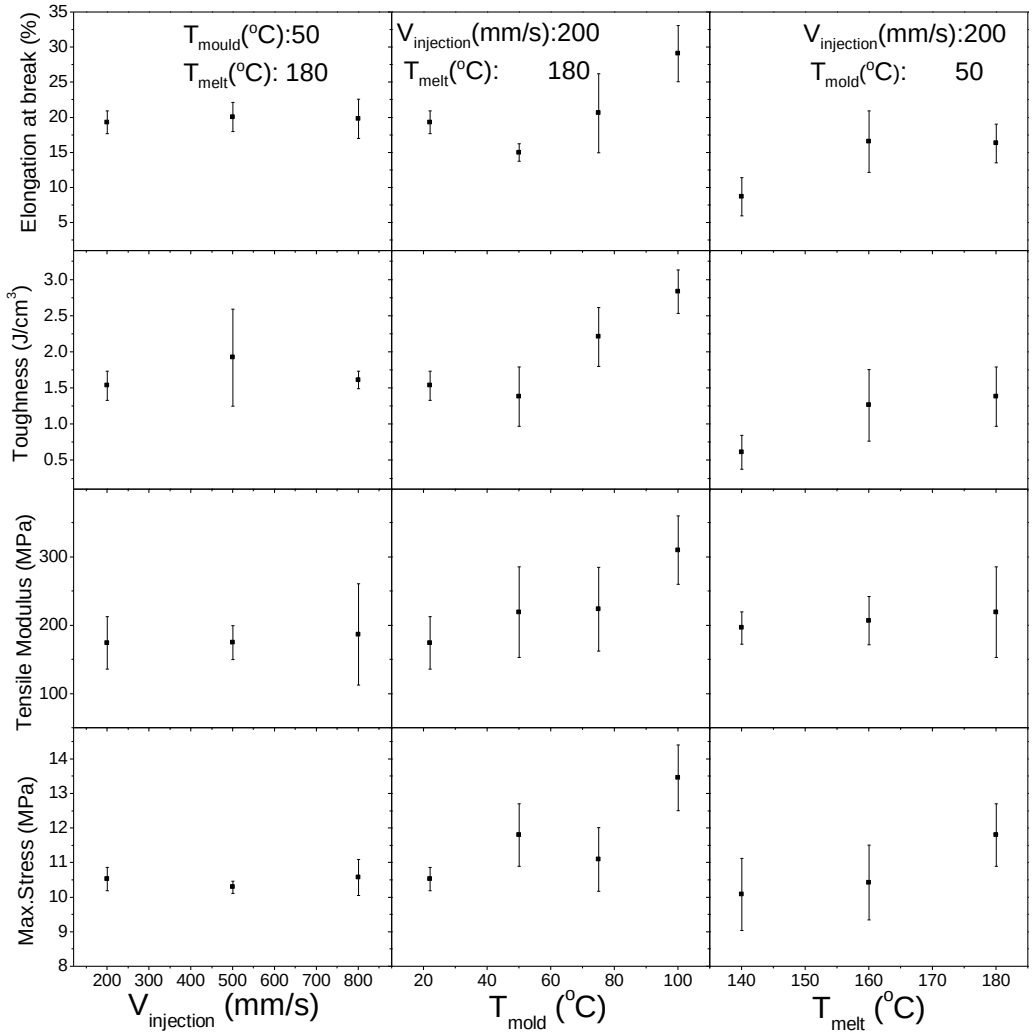

Figure 14 Tensile mechanical parameters for molded samples produced at different injection velocities (left column), mold temperatures (middle column), and melt temperatures (right column). The data are averaged over at least four repeated tests.

CONCLUSION

We have elucidated the role of injection velocity, mold temperature, and melt temperature in the microstructure and orientation distribution of microinjection molded polyethylene with a weld line. SAXS results indicate that the structural parameters at the lamellar level are affected by the injection speed and melt temperature only slightly but by the mold temperature quite markedly. The total thickness of the oriented layers, as can be assessed from the molecular orientation distribution along the thickness of molded samples, decreases with an increase of both mold temperature and melt

temperature, which is due to a relaxation of sheared chains at high temperatures and a reduced viscosity in the polymer melt, respectively. In addition, it was found that molecular chains in the weld line are oriented to a lesser degree with respect to the rest of the part of injection molded samples. Therefore, the degree of orientation of polymeric chains as quantified by the orientational order parameter can be employed to effectively determine the position of defects such as weld line occurred in the industrial shaping process. Furthermore, tensile stretching measurements indicate that the mechanical properties of welded samples are hardly influenced by the injection velocity, whereas the mechanical parameters are definitely linked to the mold temperature and the melt temperature.

ACKNOWLEDGMENTS

The authors acknowledge financial support from National Key R&D Program of China (2018YFB0704200), National Natural Science Foundation of China (21674119 and 21790342), Newton Advanced Fellowship of Royal Society (NA150222), and Jilin Scientific and Technological Development Program (Grant No. 20180519001JH). T. L. appreciates Karthik Nair and Cristina-Luminita Tuinea-Bobe in the University of Bradford for their kind assistance during the sample preparation.

REFERENCES

1 J. Giboz, T. Copponnex, P. Mele. *J. Micromech. Microeng.* **2007**, *17*(6), R96.

2 U. M. Attia, S. Marson, J. R. Alcock. *Microfluid. Nanofluid.* **2009**, *7*(1), 1.

3 C. Yang, X.-H. Yin, G.-M. Cheng. *J. Micromech. Microeng.* **2013**, *23*(9), 093001.

4 T. Nguyen-Chung. *Rheol. Acta* **2004**, *43*(3), 240.

5 S. G. Kim, N. P. Suh. *Polym. Eng. Sci.* **1986**, *26*(17), 1200.

6 S. Fellahi, A. Meddad, B. Fisa, B. Favis. *Adv. Polym. Tech.* **1995**, *14*(3), 169.

7 D. F. Mielewski, D. Bauer, P. Schmitz, H. Van Oene. *Polym. Eng. Sci.* **1998**, *38*(12), 2020.

8 J. K. Kim, J. H. Song, S. T. Chung, T. H. Kwon. *Polym. Eng. Sci.* **1997**, *37*(1), 228.

9 C. S. Chen, T. J. Chen, R. D. Chien, S. C. Chen. *Int. Commun. Heat Mass Transfer* **2007**, *34*(4), 448.

10 S. C. Chen, H. M. Li, P. L. Su, C. S. Hu. *J. Reinf. Plast. Compos.* **2009**, *28*(18), 2197.

11 L. Xie, G. Ziegmann. *Microsyst. Technol.* **2009**, *15*(9), 1427.

12 L. Xie, G. Ziegmann, M. Hlavac, R. Wittmer. *Microsyst. Technol.* **2009**, *15*(7), 1031.

13 A. Bongiorno, C. Pagano, S. Agnelli, F. Baldi, I. Fassi. *AIP Conf. Proc.* **2016**, *1713*, 120006.

14 J. Kim, H. Kim, D. Lee. *Mater. Res. Innovations* **2011**, *15*, S303.

15 J. M. Park, S. J. Jeong, S. J. Park. *J. Manuf. Sci. Eng.* **2012**, *134*(1), 014501.

16 X. P. Li, N. N. Gong, G. M. Chang. *Appl. Mech. Mater.* **2013**, *275-277*, 2210.

17 K. Tomari, H. Takashima, H. Hamada. *Adv. Polym. Tech.* **1995**, *14*(1), 25.

18 K. Tomari, T. Harada, Z. Maekawa, H. Hamada, A. Hamamoto. *Kobunshi Ronbunshu* **1992**, *49*(7), 591.

19 S. Shi, K. Zhao, L. Wang, B. Lu, G. Zheng. *J. Macromol. Sci., Phys.* **2019**, *58*(1), 28.

20 J. Healy, G. H. Edward, R. B. Knott. *J. Appl. Crystallogr.* **2007**, *40*, s393.

21 H. Granlund, J. B. Floystad, M. Esmaeili, E. T. Bakken, M. Bech, P. E. Vullum, E. Andreassen, D. W. Breiby. *Polymer* **2013**, *54*(7), 1867.

22 H. Granlund, E. Andreassen, E. T. B. Skjonsfjell, K. Hoydalsvik, A. Diaz, D. W. Breiby. *J. Polym. Sci., Part B: Polym. Phys.* **2014**, *52*(17), 1157.

23 Y. Ulcer, M. Cakmak, C. M. Hsiung. *J. Appl. Polym. Sci.* **1995**, *55*(8), 1241.

24 N. Murthy, C. Bednarczyk, R. Moore, D. Grubb. *J. Polym. Sci., Part B: Polym. Phys.* **1996**, *34*(5), 821.

25 Z. Y. Jiang, Y. J. Tang, J. Rieger, H. F. Enderle, D. Lilge, S. V. Roth, R. Gehrke, Z. H. Wu, Z. H. Li, X. H. Li, Y. F. Men. *Eur. Polym. J.* **2010**, *46*(9), 1866.

26 P. H. Hermans, P. Platzeck. *Kolloid Z.* **1939**, *88*, 68.

27 M. Polanyi. *Z. Phys.* **1921**, *7*, 149.

28 Z. Y. Jiang, Y. T. Wang, L. L. Fu, B. Whiteside, J. Wyborn, K. Norris, Z. H. Wu, P. Coates, Y. F. Men. *Macromolecules* **2013**, *46*(17), 6981.

29 Y. F. Men, J. Rieger, G. Strobl. *Phys. Rev. Lett.* **2003**, *91*(9), 095502.